Supporting Information

Cyclotriveratrylene-engineered 2D conductive Metal-Organic Framework for sensitive electrochemical detection of hydrogen peroxide

Yang Li,[a] Yiqi Zhao,[a] Wanli Ma,[a] Gang Liu,[a] Baiqing Yuan*[a] and Xiaoyu Song*[b]*

[a]School of Chemistry and Chemical Engineering, Ludong University, Yantai, 264025, China.

[b]School of Chemistry and Chemical Engineering, Yantai University, Yantai, 264005, China.

E-mail: liyang2014@tju.edu.cn；baiqingyuan1981@126.com; xiaoyusong@ytu.edu.cn

Contents

Section 1. Materials and Methods

$NaNO_2$, NaCl, $NaNO_3$, K_2SO_4, C_2H_5OH, dopamine (DA), ascorbic acid (AA), uric acid (UA), and glucose were acquired from Sigma–Aldrich. All other chemicals used were of analytical reagent grade, and the aqueous solutions were prepared with doubly distilled water. Electrochemical experiments were performed in 0.1 M phosphate buffer solution (PBS, pH 5–8) and 0.1 M acetate buffer solution (ABS, pH 4).

^{1}H NMR was recorded on a Bruker ADVANCE III HD (400 MHz) using deuterated solvents as internal deuterium lock. Powder X-ray diffraction measurements were recorded on X-ray diffractometer (RIGAKU SMARTLAB 9 KW). The Pawley refinements were performed by the Reflex module in the Material Studio. Nitrogen adsorption and desorption isotherms were carried out with Bel Japan Inc. model BELSOPR-Max analyzer at 77 K. The samples were activated at 120 °C for 12 hours under vacuum (10^{-5} bar) prior to the gas sorption analysis. Surface areas were calculated from the nitrogen adsorption data. Fourier transform infrared spectroscopy (FT-IR) was carried out with a Bruker Alpha spectrometer. Transmission electron microscopy (TEM) imaging was performed on a JEOL model JEM-2100 at 100 kV. Field emission scanning electron microscopies (FE-SEM) were carried out using a Hitachi Limited model SU8010 microscope operating at an accelerating voltage of 5.0 kV. Conductivity measurements were performed using a physical property measurement system (PPMS, Quantum Design).

Section 2. Synthesis and Preparation

Synthesis of hexahydroxycyclotribenzylene (HCB).

Hexahydroxycyclotribenzylene (HCB) was synthesized according to previous reported procedures.[S1]

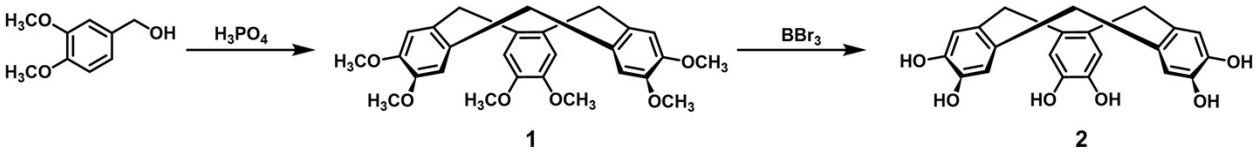

1 2

Scheme S1. Synthesis of HCB.

Cyclotriveratrylene (CTV) (1). 3,4-Dimethoxybenzyl alcohol (1.0 g, 6 μmol) was placed in a reaction tube and heated in an oil bath to 80 ℃. A few drops of H_3PO_4 were added and the reaction mixture was stirred for 5 h. After cooling down to room temperature, the mixture was then treated with methanol (10 mL). The crude solid was collected by filtration and recrystallized from dichloromethane/methanol to yield 0.27 g (31%) of pure white crystal. ^{1}H NMR (400 MHz, $CDCl_3$): δ (ppm) 6.83 (s, 6 H), 4.78 (d, 3H), 3.84 (s, 18 H), 3.56 (d, 3H).

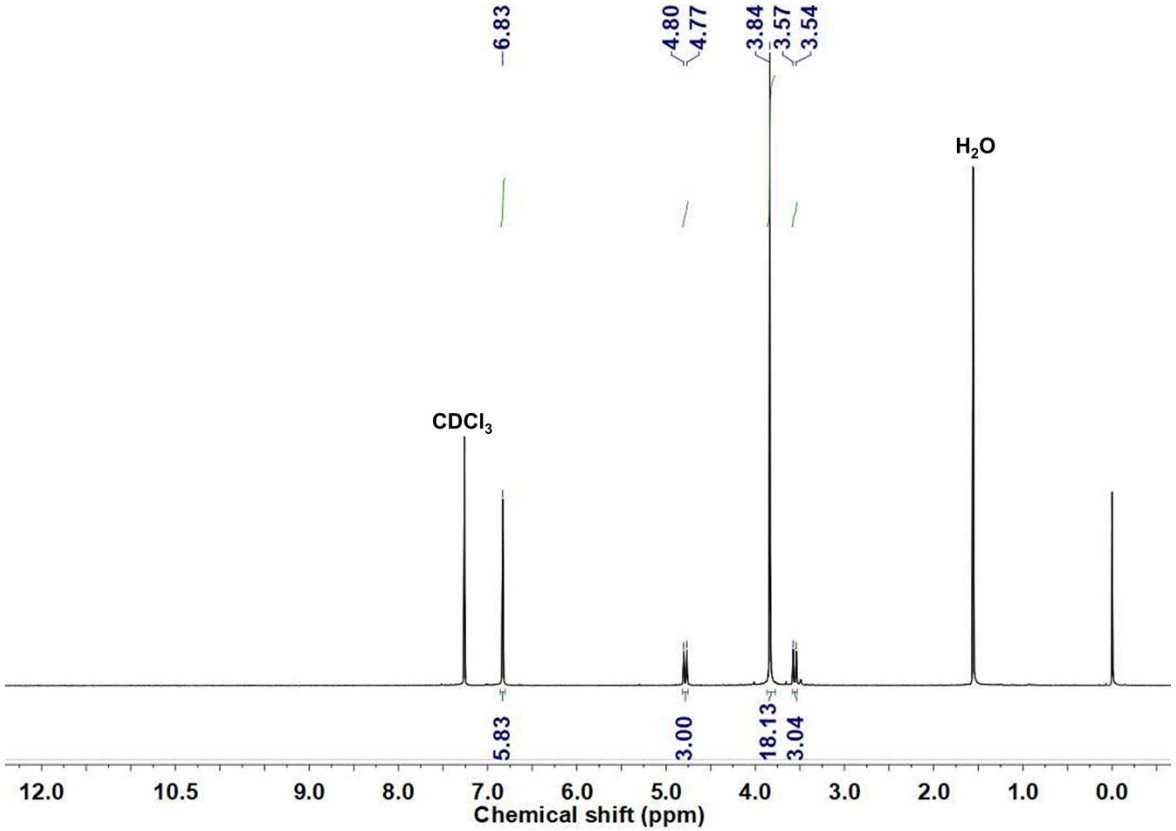

Figure S1. ^{1}H NMR spectrum of **CTV** (298 K, 400 MHz, $CDCl_3$).

Hexahydroxycyclotribenzylene (HCB) (2). CTV (0.25 g, 0.5 mmol) was dissolved in dry dichloromethane in a reaction tube under nitrogen. BBr_3 in dry dichloromethane solution (*v*/*v* = 1:4) was added dropwise to the reaction mixture at 0 ℃. The slightly purple reaction mixture was stirred at 0 °C for 50 min, at RT for 30 min, and then refluxed for 12 h. After cooling down to room temperature, the mixture was then treated with ice water (10 mL). The resulting slurry was filtered and washed with H_2O. The crude wet solid was recrystallized from CH_3OH and H_2O to yield 0.1 g (55%) of pale solid. ^{1}H NMR (400 MHz, DMSO-d_6): δ (ppm) 8.56 (s, 6 H), 6.65 (s, 6 H), 4.48 (d, 3H), 3.19 (d, 3H).

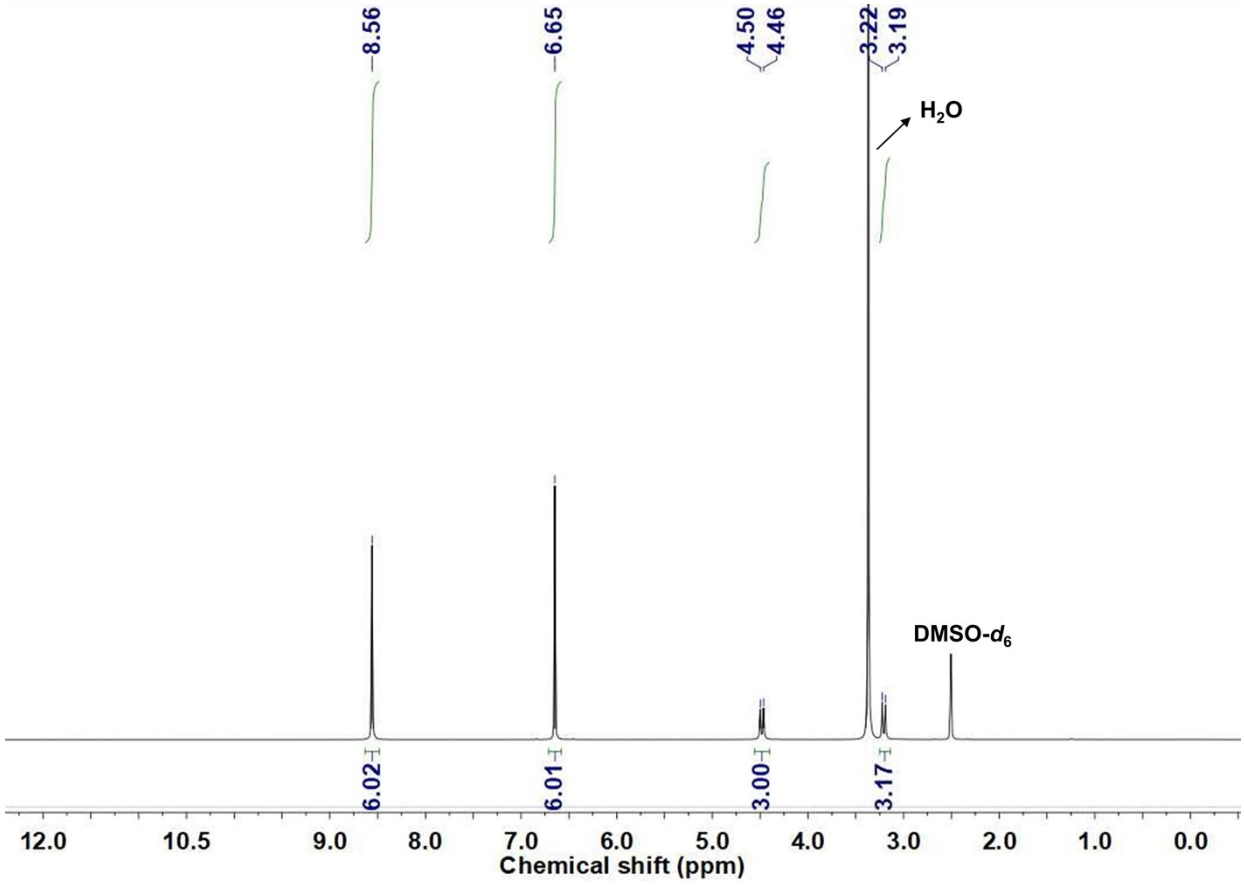

Figure S2. ^{1}H NMR spectrum of **HCB** (298 K, 400 MHz, DMSO-d_6).

Synthesis of HCB-Cu

In a typical reaction, HCB (5.5 mg, 0.015 mmol) was suspended in a mixture of H_2O (1.3 mL) and N,N-dimethylformamide (0.3 mL) in a sealed glass bottle and sonicated for 5 min. Copper acetate ($Cu(OAc)_2 \cdot H_2O$, 10.5 mg, 0.053 mmol) was dissolved in a small amount of water (0.5 mL) and added slowly into the solution of HCB. The reaction mixture was further sonicated for 30 min.

The vial was carefully sealed and heated at 75 °C for 16 h. After cooling to room temperature, the dark blue powder was isolated by centrifugation and washed with N,N-dimethylformamide, H_2O and acetone. The sample of HCB-Cu was obtained by vacuum drying overnight at 60 °C.

Section 3. Apparatus and Characterization

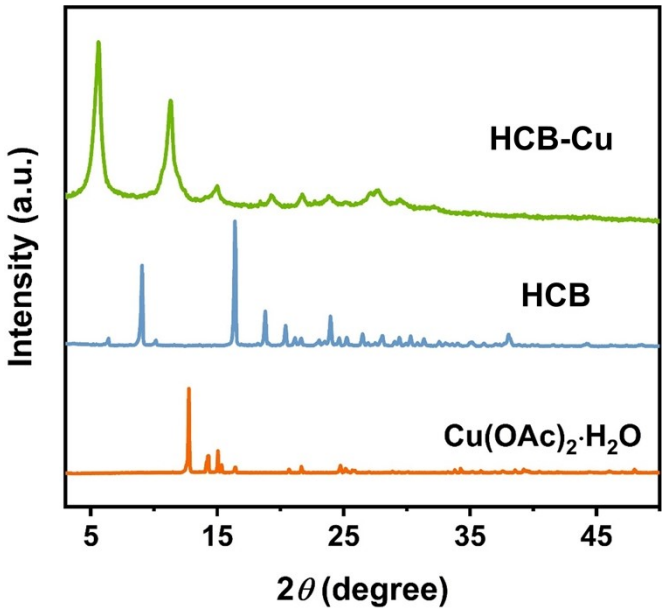

Figure S3. PXRD patterns of HCB-Cu, HCB and $Cu(OAc)_2 \cdot H_2O$.

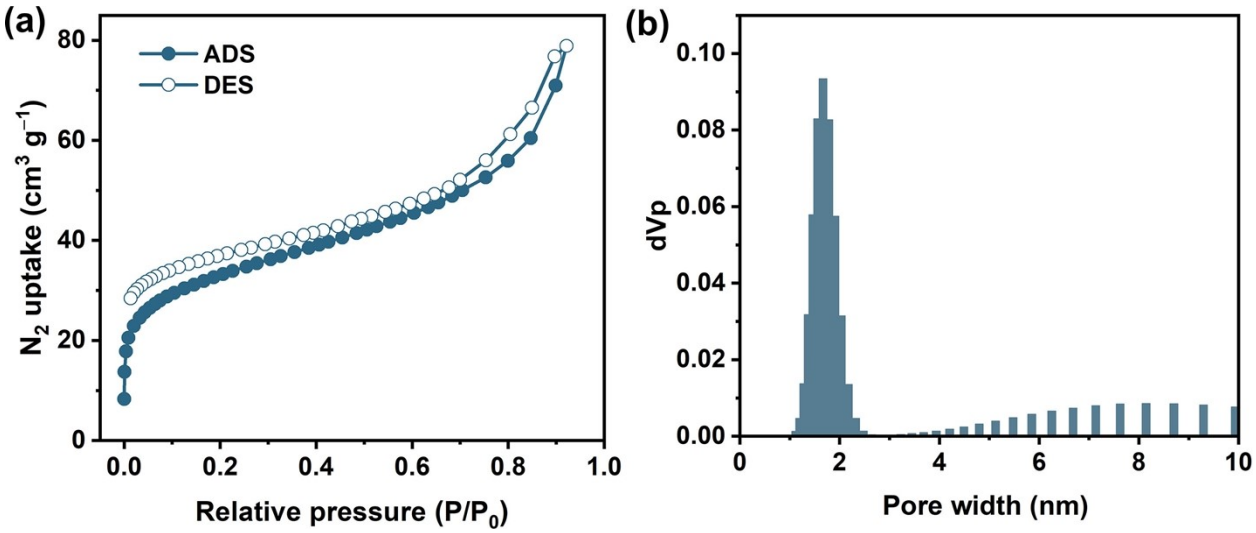

Figure S4. (a) Nitrogen adsorption-desorption isotherms of HCB-Cu at 77 K; (b) Pore size distribution of HCB-Cu.

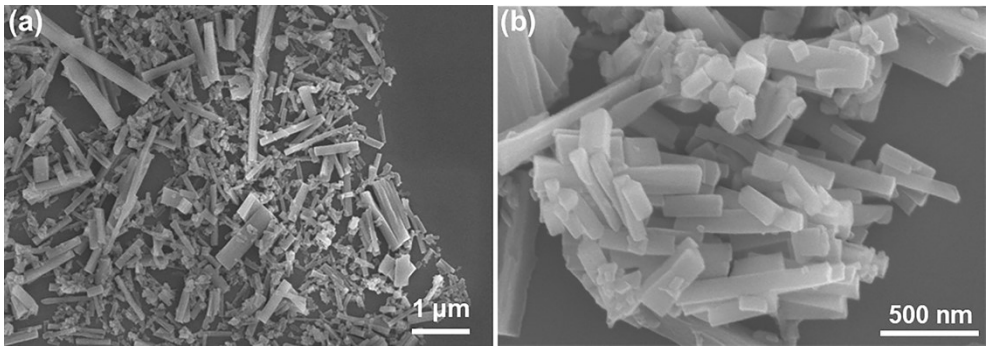

Figure S5. (a) Low-resolution and (b) high-resolution SEM images of HCB-Cu.

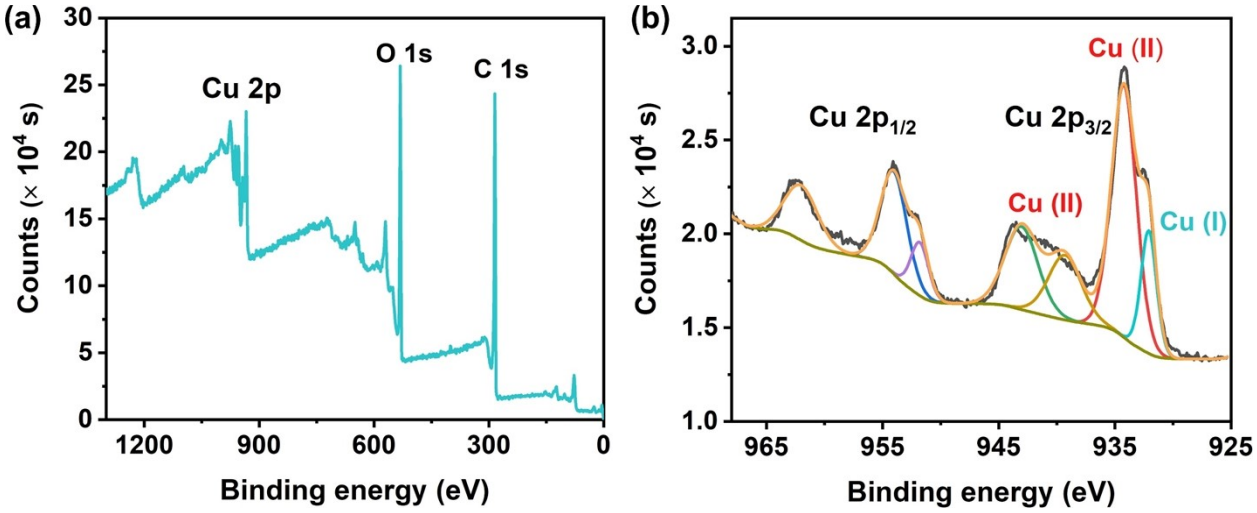

Figure S6. (a) XPS survey spectrum of HCB-Cu; (b) XPS high-resolution spectrum of Cu 2p. The obtained data were charge-corrected with the binding energy of C 1s with externally contaminated carbon (284.8 eV), and the high-resolution spectra of Cu elements in HCB-Cu were peak-split by Avantage software.

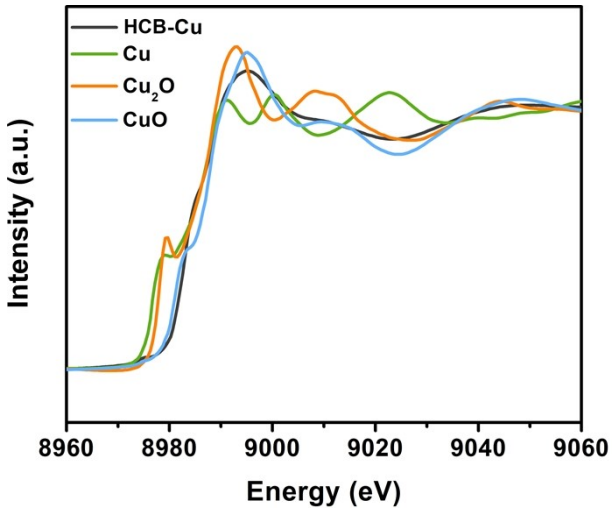

Figure S7. Cu K-edge XANES spectra of Cu foil, Cu_2O, CuO and HCB-Cu.

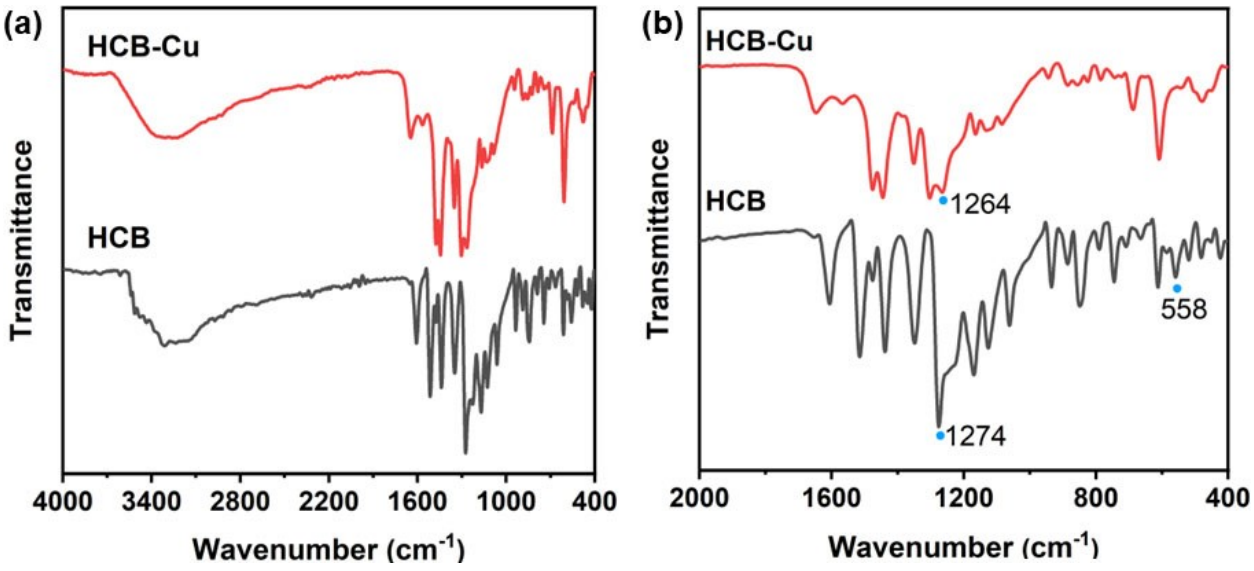

Figure S8. (a) FT-IR absorption spectra of HCB-Cu (red line) and HCB ligand (black line); (b) Magnified view of the fingerprint region.

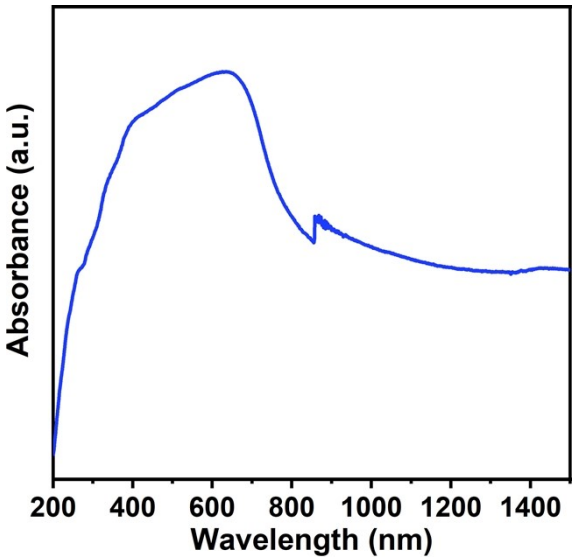

Figure S9. The solid-state diffuse reflectance of UV-vis absorption spectrum of HCB-Cu powder.

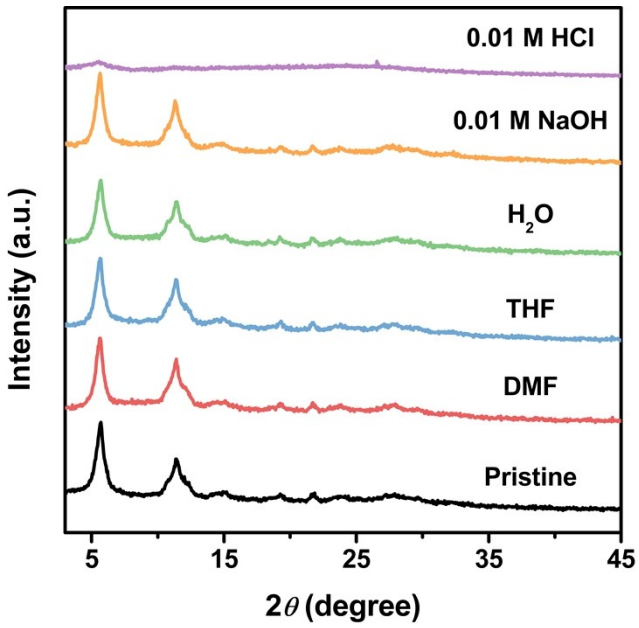

Figure S10. PXRD patterns of HCB-Cu after immersing in different solvents for three days.

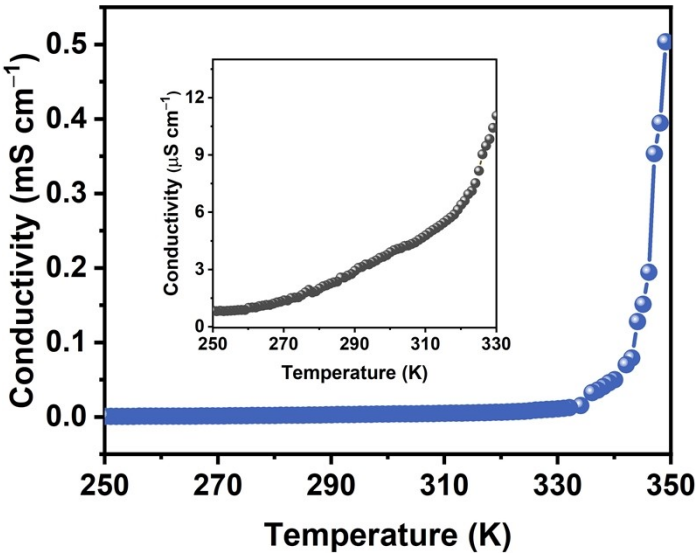

Figure S11. Temperature-dependent conductivity of HCB-Cu measured by van der Pauw method (inset: magnified region ranging from 250 to 330 K).

Electrochemical pretreatment and characterization. A CHI 750E electrochemical workstation was used to perform all the electrochemical experiments with the conventional three electrode system which was composed of HCB-Cu modified glassy carbon electrode (GCE) or bare GCE working electrode, platinum coil auxiliary electrode, and Ag/AgCl (saturated KCl) reference electrode. The GCE (3 mm diameter) was polished on suede with 1.0, 0.3, and 0.05 μm Al_2O_3 powder before electrode modification, then rinsed with deionized water, sonicated in water and ethanol, and dried for later use. Subsequently, two distinct electrochemical activation protocols were implemented: (1) single-step anodic polarization in pH 7.0 PBS at 1.75 V for 500 s (designated as O-GCE) or (2) a sequential anodic-cathodic treatment comprising primary anodic oxidation followed by cathodic reduction in pH 4.0 ABS at -0.85 V for 500 s (designated as OR-GCE).[S2] To evaluate the effect of pretreatment on the electrode surface properties, cyclic voltammetry (CV) was performed using 5 mM $K_3[Fe(CN)_6]/K_4[Fe(CN)_6]$ as a redox probe. Electrochemical impedance spectroscopy (EIS) measurements were also conducted in the same solution. Compared to the bare GCE, the O-GCE exhibits a reduced peak current. This is because

the O-GCE possesses more abundant oxo-functionalized groups, such as negatively charged carboxyl groups, which electrostatically repel the $[Fe(CN)_6]^{3-/4-}$ anions.[S3] In contrast, the OR-GCE demonstrates improved reversibility and a higher current response, indicating enhanced catalytic activity and conductivity. Consistently, the EIS data also indicate the same trend in conductivity (OR-GCE > GCE > O-GCE), in full agreement with the CV results.

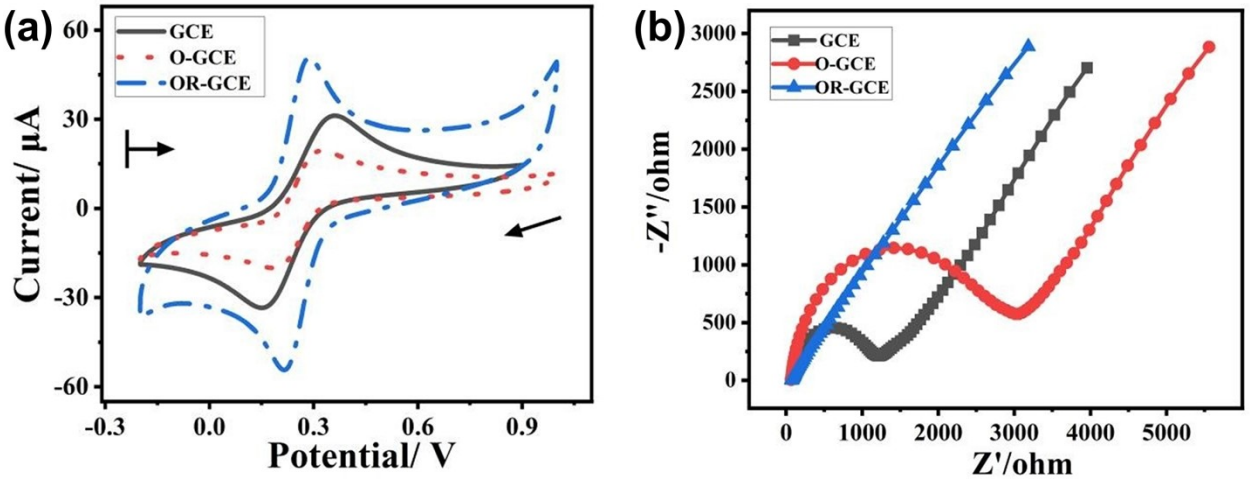

Figure S12. (a) CVs for GCE, O-GCE , and OR-GCE in 5 mM $[Fe(CN)_6]^{3-/4-}$; (b) Nyquist diagrams for GCE, O-GCE, and OR-GCE in 5 mM $[Fe(CN)_6]^{3-/4-}$.

3.0 mg HCB-Cu was dispersed in 1.0 mL of deionized water and sonicated for 30 min to obtain an HCB-Cu dispersion at a concentration of 3.0 mg mL^{-1}. A 5.0 μL droplet of HCB-Cu suspension was prepared by placing a droplet of HCB-Cu on a cleaned GCE or O-GCE or OR-GCE and drying it at room temperature (named HCB-Cu/GCE, HCB-Cu/O-GCE, HCB-Cu/OR-GCE).

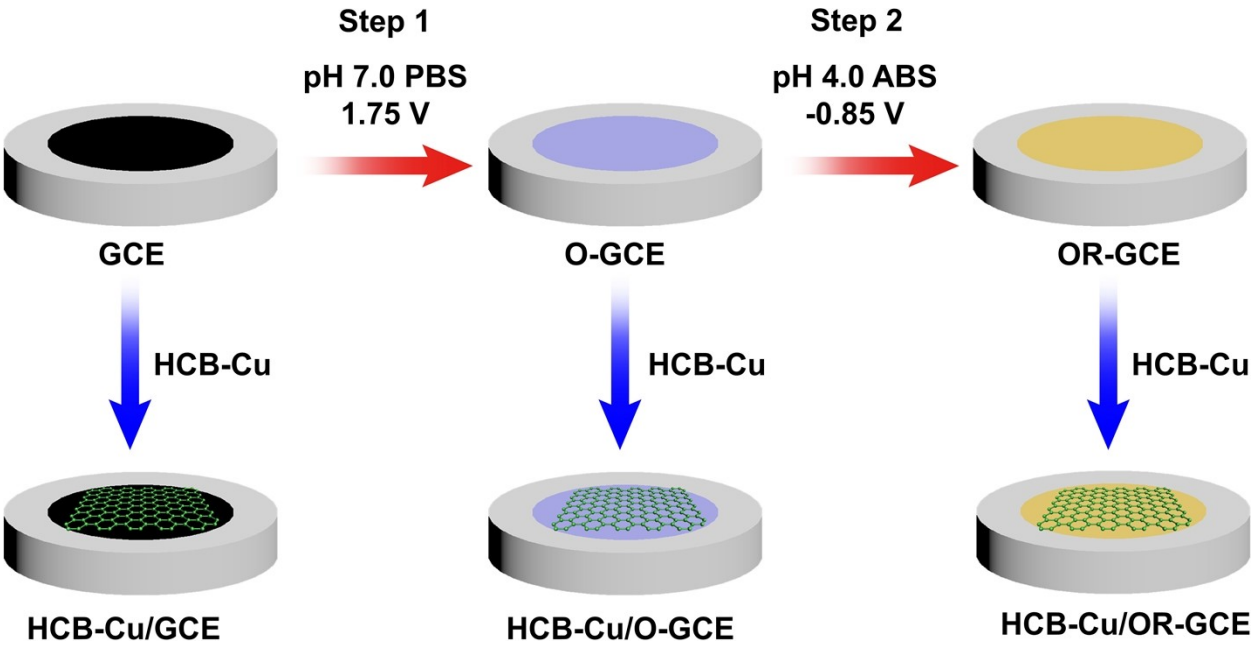

Scheme S2. Schematic diagram of the preparation of modified electrodes.

XPS is extremely sensitive to the surface (~10 nm) and may detect copper species associated with surface defects, partial reduction, or alterations in the ligand environment. In contrast, XANES reflects the overall average chemical state of the material and is sensitive to the coordination environment. Therefore, this discrepancy strongly suggests the existence of local, non-steady-state Cu(I) species in the surface or near-surface region of the MOF (which may also be induced by X-rays or vacuum, or inherently exist), while the bulk matrix of the material remains predominantly Cu(II). These surface Cu(I) sites may exhibit peroxidase-like activity, potentially contributing to driving the catalytic cycle for H_2O_2 reduction: The reversible interconversion between Cu(I) and Cu(II) driven by electrode potential. During H_2O_2 reduction at negative potentials, Cu(II) sites in the MOF framework can be reduced to Cu(I), which subsequently activate and reduce H_2O_2, regenerating Cu(II) and completing the catalytic cycle.[S4]

Section 4. Calculated Atomic Coordinates of AA-Stacking Mode

Table S1. Atomic coordinates of AA-stacking mode of HCB-Cu using forcite method.

Space group: *P*-3M1 **$a = b = 19.2181$ Å, and $c = 4.5303$ Å** **$\alpha = \beta = 90°$, $\gamma = 120°$**			
	X	Y	Z
C1	0.22206	0.57396	-0.24348
C3	0.27978	0.55955	-0.42458
C10	0.34457	0.51015	-0.06745
C11	0.40816	0.51993	0.10917
H31	0.29638	0.59276	-0.63431
H32	0.24806	0.49612	-0.50215
O22	0.05796	0.5989	0.29274
Cu23	0	0.5	0.5
H37	0.28913	0.45301	-0.06426

Table S2. Analytical properties comparison of various H_2O_2 sensors.

Modified electrodes	Linear range (μM)	Detection limit (μM)	Sensitivity (μA mM^{-1} cm^{-2})	Ref.
NCST-1	5-18000	6.86	52.55	[S5]
Co-MOF	5-9000	3.76	83.10	[S6]
2D Cu-TCPP/MWCNTs	1-8159	0.70	157	[S7]
GN@FeOOH	0.25-1200	0.08	265.7	[S8]
Ni_7S_6	5-3700	0.15	271.9	[S9]
HCB-Cu	**10-3680**	**5.8 (10^a)**	**365.04**	**This work**
2D-CoMOF	5-1000, 1000-12000	38.1	570, 395	[S10]

a: practical detection limit

Section 5. Supporting References

S1. X. Ouyang, R. Liang, Y. Hu, G. Li, C. Hu and Q. Zhong, *J. Chromatogr. A*, 2021, **1656**, 462538.

S2. Y. Yi, G. Weinberg, M. Prenzel, M. Greiner, S. Heumann, S. Becker and R. Schlögl, *Catal. Today*, 2017, **295**, 32-40.

S3. S. H. Choudhury, Y. Ding, Y. Yi, C. Rohner, W. Frandsen, T. Lunkenbein, M. Greiner, R. Schlögl and S. Heumann, *ChemElectroChem*, 2022, **9**, e202200637.

S4. L. Jiang, H. Wang, Z. Rao, J. Zhu, G. Li, Q. Huang, Z. Wang and H. Liu, *J. Colloid Interface Sci.*, 2022, **622**, 871-879.

S5. Q.-Q. Xiao, D. Liu, Y.-L. Wei and G.-H. Cui, *Polyhedron*, 2019, **158**, 342-351.

S6. L. Yang, C. Xu, W. Ye and W. Liu, *Sens. Actuators B*, 2015, **215**, 489-496.

S7. C. Wang, S. Huang, L. Luo, Y. Zhou, X. Lu, G. Zhang, H. Ye, J. Gu and F. Cao, *J. Electroanal. Chem.*, 2019, **835**, 178-185.

S8. X. Chen, J. Gao, G. Zhao and C. Wu, *Sens. Actuators B*, 2020, **313**, 128038.

S9. W. Wu, Y. Li, J. Jin, H. Wu, S. Wang and Q. Xia, *Sens. Actuators B*, 2016, **232**, 633-641.

S10. A. Portorreal-Bottier, S. Gutiérrez-Tarriño, J. J. Calvente, R. Andreu, E. Roldán, P. Oña-Burgos and J. L. Olloqui-Sariego, *Sens. Actuators B*, 2022, **368**, 132129.